Towards LES-RANS/LES coupling for simulation of a wind turbine rotor in a nocturnal atmospheric condition

Journal of Physics: Conference Series **2767** (2024) 022009 doi:10.1088/1742-6596/2767/2/022009

Towards LES-RANS/LES coupling for simulation of a wind turbine rotor in a nocturnal atmospheric condition

Manfred Imiela[1], Linus Wrba[2], Axel Probst[1], Galih Bangga[3], Antonia Englberger[2]

[1] Institute of Aerodynamics and Flow Technology, German Aerospace Center (DLR)
[2] Institute of Atmospheric Physics, German Aerospace Center (DLR)
[3] Turbine Engineering, Bladed Team, Det Norske Veritas (DNV)

E-mail: manfred.imiela@dlr.de

Abstract. A segregated approach with either synthetically generated velocity fluctuations or a precursor Large-Eddy Simulation (LES) of the atmospheric boundary layer (ABL) and a subsequent hybrid RANS/LES (HRLS) of the resolved rotor is presented in this paper. At first the approach is validated with synthetically generated velocity fluctuations that resemble neutrally stratified conditions. Subsequently the same turbine is artificially exposed to a stably stratified atmospheric inflow (nocturnal boundary layer) with a comparable mean velocity but different shear and veer characteristics. The HRLS simulations with the neutrally stratified and stably stratified inflow are compared to LESs with an implemented actuator disc (AD) model. The presented work is a first important step towards a digital twin for research wind parks.

1. Introduction

During the last decade unsteady Reynolds-averaged Navier-Stokes (URANS) simulations of a fully resolved wind turbine with laminar inflow have become state of the art. Full size wind turbines, however, are exposed to the turbulent flow conditions of the atmosphere. While LES in combination with the AD have already widely been applied for rotor simulations in turbulent atmospheric flows, e.g. [1, 10, 19], an LES of the atmosphere including a fully resolved turbine is prohibitively expensive. The modelling of the rotor with an AD model, however, leads to less accurate results regarding rotor loads and the near wake. Therefore a segregated approach with either synthetically generated velocity fluctuations or a precursor LES of the ABL and a subsequent HRLS simulation of the resolved rotor such as in Wenz et al. [20] has been adopted in this paper. At first, the HRLS model is validated with experimental data of the implemented rotor for a flow with synthetically generated velocity fluctuations that resembles neutrally stratified conditions. The results from the HRLS approach are compared to an LES with an AD in order to distinguish the differences in the developed wake behind the rotor. Additionally, the flow through the turbine is simulated with both numeric approaches using turbulent fluctuations from a nocturnal atmospheric precursor simulation. This precursor simulation naturally comprises shear and veer in the atmosphere, the latter resulting from the Coriolis force in combination with surface friction. This so called Ekman spiral is of special interest since it varies the angle of attack over one revolution at a fixed radial position. The differences of the developed wake in the simulations with the HRLS model and the LES + AD approach are compared in detail and the advantages and drawbacks are presented, respectively.

2. Methodology

2.1. Experimental Reference Data and Mesh Setup

The DanAero wind turbine [17] serves as the reference wind turbine in the current study. The experimental field campaign has been conducted between 2007-2010 by a consortium consisting of the Technical University of Denmark (DTU) and the industrial partners Vestas, Siemens LM and DONG Energy. By that time the turbine represented an industrial state of the art turbine with a hub height of 57.19m, a rotor diameter of 80m, a tilt angle of 5° and a blade tip prebend of 1.4m.

The turbine and measurement data have been provided to the members of the IEA Task 29 phase IV in 2018. Within the work package for turbulent inflow four different measurements (see [13]) were identified during which the inflow conditions wrt the inflow direction, inflow velocity at hub height (U_{hub}), shear exponent (α), turbulence intensity (TI),length scale (L) and turbine parameters such as the rotational speed of the rotor (Ω) and blade pitch angle (θ) remained at about a constant level. The reference values of the fourth case which will be used for validation of the current HRLS approach are listed in Table 1. Note that the yaw angle is slightly varied between the validation (=VC) and the subsequent nocturnal case (=NC).

In order to be able to compare the results from the measurement and the CFD simulations, the turbulence characteristics that were present during the measurement need to be considered in the CFD simulations. This can either be done via an LES precursor simulation from which velocity fluctuations around the mean velocity can be extracted or by synthetically generating the velocity fluctuations via a Mann box using the turbulence characteristics from the measurement represented by the turbulence intensity and length scale. The methodology, dimensions, resolution and boundary conditions of the background mesh, the inflow and injection of the turbulent fluctuations is depicted in Figure 1. Regardless of the generation method the turbulent velocity fluctuations are superimposed in the subsequent HRLS on the mean wind velocity at $X = -320m$ (i.e. upstream of the turbine) by a momentum source term (named body force = bf). The implementation is done as in Troldborg et al. [18] using the following equation:

Parameter	Value
$U_{hub}[m/s]$	9.792
$\alpha_S[-]$	0.249
$TI[\%]$	3.66
$L[m]$	32.026
$n[RPM]$	16.2
$Pitch[°]$	-4.75
$Yaw[°]$	-6.02 (VC)/-10.0 (NC)

Table 1: Reference Flow Quantities

Mesh Component	Mesh Points
Background	99.3e6
Rotor Refinement	2.4e6
Hub Refinement	0.9e6
Hub	3*0.3e6
Blade	3*8.9e6
Total	130.2e6

Table 2: Mesh Resolution

$$f_{bf} = \frac{\rho u_i'}{\Delta x_n}\left(u_n + \frac{1}{2}u_n'\right) \tag{1}$$

with ρ being the density, Δx_n the grid spacing normal to the actuator, u_i' the component of the fluctuation in the respective axis direction, u_n being the normal component of the mean velocity and u_n' the normal component of the fluctuation velocity. For both simulations (validation and nocturnal case) the mean wind profile is fed in at the inflow of the domain. While in the validation case the wind profile is obtained by the simple power law, sixth order piecewise polynomial functions are applied in the nocturnal case. Both simulations are conducted over 45 revolutions of which 20 revolutions are used for initialization and the latter 25 revolutions for the analysis of the forces and wakes.

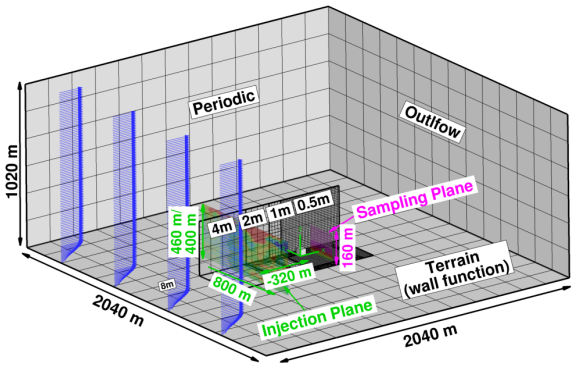

Figure 1: Dimensions, resolution, mean boundary layer profile, injection, sampling plane and boundary conditions of the background mesh (mesh resolution and boundary layer profile coarsened for visibility).

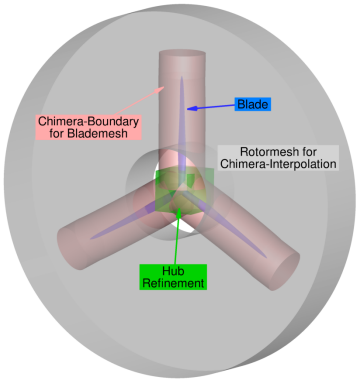

Figure 2: Mesh components of the rotor: Surfaces: Blade (blue), Chimera boundary of the blade mesh (pink), Chimera boundary of the hub refinement (green), Chimera boundary of the rotor mesh refinement (gray).

Due to the high complexity of the HRLS the mesh setup was kept fairly simple. Therefore only the rotor was modelled and the nacelle and tower were omitted. The rotation of the rotor in the stationary background grid is achieved via the Chimera technique. The domain size of the background grid was chosen to be [$2048m$ x $2048m$ x $1024m$] in order to minimize any influences from the boundaries as much as possible. The background grid consists of a staggered cartesian grid sequence ranging from 8m at the inflow to 0.5m near the rotor. For the FLOWer ([7]) background mesh no gaps exist between the various cartesian regions. For TAU small transition regions with unstructured elements (i.e. prisms and tetrahedra) between the cartesian regions had to be integrated. For TAU the wall function of Knopp [6] is applied on the Terrain surface (see Figure 1) in order to ease the resolution requirements in the vicinity of the ground.
For the blade mesh a convergence study was performed previously for the 10 MW generic AVATAR rotor [2]. A grid convergence index of 0.5% was achieved for the fine grid. The mesh features an O-type topology with [256 x 128 x 200] grid cells in chordwise, normal and radial direction. Half of the points in the wall normal direction are located in the boundary layer guaranteeing an adequate resolution of the turbulent flow without wall function. The blade meshes are embedded in a rotating disc and hub refinement ensuring similar mesh resolutions in the overlapping regions. The hub, blade and refinement meshes are shown in Figure 2. The total grid comprises app. 130 million grid points. The contribution of each individual component mesh is listed in Table 2. Regarding the reference data, the methodology, mesh setup and synthetic velocity fluctuation additional information can be found in [13] and [3].

2.2. Synthetic Velocity Fluctuations

The turbulent fluctuations for the validation case have been generated with PROFGEN [13]. The size of the Mann box was chosen to be [$800m$ x $460m$ x $720m$] with a grid spacing in lateral (ΔY) and wall normal direction (ΔZ) of $4m$. The size in flow direction (X) determines the temporal length of the Mann box which in this case equals to $T_{Mann} = 73.529s$. Note that the turbulent Mann box is generated with periodicity, so that it can be reused if the simulation time exceeds the length of the Mann box such as in this case. The wind turbine class was assumed to be 1A. To match the atmospheric conditions as required in the IEC61400-1 a non-isotropic turbulence was created. Therefore, the stretching factor was chosen to be $\Gamma = 3.9$ to approximate the Kaimal spectral model.

2.3. LES

The atmospheric simulation to generate stably-stratified turbulent inflow data for the HRLS model as well as the LES with the DanAero wind turbine are conducted with the geophysical flow solver EULAG [12]. The set of non-hydrostatic Boussinesq equations are solved for the Cartesian velocity components $\mathbf{v} = (u, v, w)$ and the potential temperature perturbation Θ'. The transport algorithm MPDATA established in this numerical model is a finite difference algorithm for approximating the advective terms in the fluid equations [16]. The LESs are conducted with a turbulence kinetic energy closure.

2.3.1. LES of the Atmospheric Boundary Layer

The precursor LES represents a nighttime situation of an idealized diurnal cycle with atmospheric conditions for Germany by the definition of the Coriolis force, the temperature profile and the heat flux. The surface is prescribed by a Neumann boundary condition with a negative heat flux. The boundary condition at the surface is partial slip with a drag coefficient. The resulting surface friction and the Coriolis force lead to the characteristic mean wind profiles with shear and veer. The turbulence structure in the resulting stably-stratified atmosphere shows elongated patches which differ strongly in comparison to a neutral stratification. A detailed description of the numerical setup for this stable boundary layer can be found in [5].

2.3.2. Parameterization of the rotor

The rotor parameterization in the LES model follows the Blade Element Momentum Theory as a rotating AD [10] combined with the immersed boundary method. The aerodynamic polar data for the blade use the hybrid 3D CFD synthesized data to obtain best consistency with fully resolved calculations as suggested in [4]. The dedicated polar data was obtained from the IEA Wind Task 29 comparison round [13]. The generated forces of the rotor blades on the flow are taken into account in the momentum equation in the flow solver EULAG.

2.4. Near-field rotor simulation (HRLS)

2.4.1. HRLS with FLOWer

The reference cases were simulated using the structured compressible flow solver FLOWer. The code was originally developed at DLR and has been extensively extended for wind energy applications at IAG in the last decades. The simulations adopted a fully resolved grid approach together with the Chimera overlapping mesh technique. The solutions were provided using a hybrid RANS/LES method in combination with the 5th order WENO scheme for resolving the wake structures and the 2nd order accuracy near the wall surfaces. The calculations in FLOWer were done at the center of the grid cell. The time marching was provided using an implicit time stepping with a 2° of rotor rotation per physical time step size.

2.4.2. HRLS with TAU

The simulations of the fully-resolved rotor in turbulent inflow are conducted with the unstructured compressible flow solver DLR-TAU [14] and a hybrid RANS/LES method. TAU employs a 2nd-order finite-volume method on grids with mixed elements (e.g. tetrahedra, hexahedra, prisms) which is suited for complex, moving geometries. The time marching is achieved by a dual time stepping scheme using a 1° azimuthal resolution. Relative motion such as rotor rotation is realized by transferring the flow variables between separate overlapping grid blocks via interpolation (*Chimera* technique). To ensure sufficient numerical accuracy of resolved turbulent structures, a low-dissipation low-dispersion scheme (LD2) [8] is used in hybrid RANS/LES simulations. In the present work a hybrid form of this scheme is applied [11] which restricts the LD2 scheme to the LES regions, retaining robustness in the RANS regions.

Turbulence modelling setup The near-field simulation setup comprises an inflow region with the prescribed ABL profile and purely modelled turbulence, employing the URANS approach with the Shear Stress Transport (=SST) two-equation turbulence model [9]. At a sufficient distance upstream of the rotor, the time- and space-resolved fluctuations from either synthetic turbulence [13] or the atmospheric LES are injected in the flow field via body forces in the momentum and energy equations. At the same position the RANS model is switched to the wall-modelled LES (WMLES) mode of the Improved Delayed Detached-Eddy Simulation (IDDES, [15]), which is the hybrid RANS/LES model used in this work. It replaces the integral turbulent (i.e. RANS) length scale, l_{RANS}, in the dissipation term of the underlying RANS model by a *hybrid* length scale, reading:

$$l_{hyb} = \tilde{f}_d \left(1 + f_e\right) l_{\mathrm{RANS}} + \left(1 - \tilde{f}_d\right) l_{\mathrm{LES}} \quad . \tag{2}$$

The function $\tilde{f}_d = \max\left\{\left(1 - f_{dt}\right), f_B\right\}$ performs an automatic switching between the different modelling modes of IDDES, i.e. RANS mode ($l_{hyb} \equiv l_{\mathrm{RANS}}$), pure LES mode ($l_{hyb} \equiv l_{\mathrm{LES}} = C_{\mathrm{DES}}\Delta_{\mathrm{IDDES}}$), and the mentioned WMLES mode which actually blends RANS mode in the near-wall region with LES mode in the outer boundary layer. The rather complex, grid- and geometry-dependent expression for the LES filter width:

$$\Delta_{\mathrm{IDDES}} = \min\left\{\max\left[C_w \cdot d_w, C_w \cdot h_{\max}, h_{wn}\right], h_{\max}\right\} \ , \quad \text{with: } C_w = 0.15 \ , \tag{3}$$

allows using a unique LES calibration coefficient C_{DES} for both wall-bounded and free turbulent flow. While f_{dt} and f_B depend on local grid and flow properties, the additional *elevating* function f_e is designed to avoid a damping of the modelled Reynolds stresses in the wall-parallel interface region between the RANS and LES, thus reducing the log-layer mismatch often observed in WMLES (cf. [15] for details). To realise the *embedded* WMLES in the surrounding of the rotor, the function f_{dt} that enters Eq. (2) is manually set to 1 in the region ranging from the injection plane of resolved turbulence up to about 3 diameters downstream of the rotor. In the vicinity of the rotor-blade surface, the hybrid model is enforced to RANS mode by means of a simple wall-distance criterion, so that the rotor boundary layer is fully covered by the SST model. Otherwise, it would not be affordable to resolve both the relatively low-frequency motion of the ABL and the much smaller turbulent scales of the rotor boundary layer by WMLES simultaneously.

3. Results

3.1. Verification and Validation

For validation of the HRLS approach the FLOWer and TAU results are compared to the experiments labeled as fourth reference case in [13] or as turbulent sheared case in [3]. Figure 3 shows the mean streamwise flow velocity ($\overline{u}$) and the turbulent intensity (TI_x) from the **empty box simulations** averaged over the last 25 rotor revolutions. Unfortunately only one experimental value exist at the metmast which is located 320m upstream of the turbine. Therefore a full validation of the mean streamwise velocity and turbulent intensity is not possible. However, under the hypothesis that the upstream influence of the turbine on the metmast measurement is negligibly small it can be stated that the simulation results are in very good agreement with the measurements. Regarding the flow velocity the TAU result even seems to fit slightly better. It was reported that there was a slight density-normalization issue in the FLOWer empty box results, but this was resolved in the rotor simulations [3]. The development of the turbulent intensity is also similar in both codes, merely the absolute value of the turbulent intensity is slightly different. While the streamwise change in the experiment cannot be assessed at all, the comparison between metmast and first output plane of the simulation (X = -240m) shows excellent agreement. Also for the vertical distribution of the velocity and turbulent

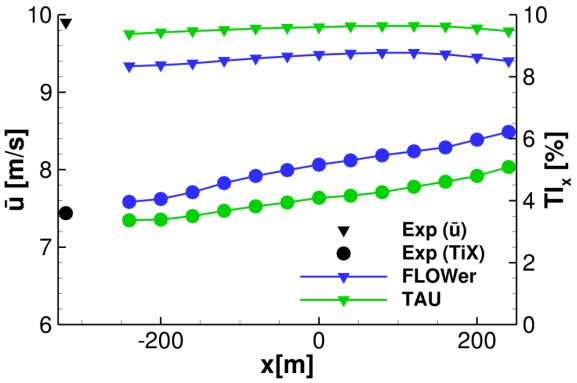

Figure 3: Mean streamwise flow velocity ($\overline{u}$: triangles) and turbulent intensity (TI_x: circles) at hub height from empty box simulation averaged over last 25 rotor revolutions. Experimental values at metmast @ X=-320m

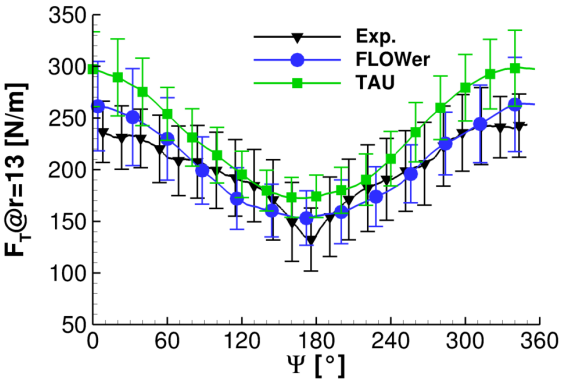

Figure 4: Tangential force at 13m radius from experiment (black triangles), FLOWer (blue circles) and TAU (green squares) averaged over last 25 rotor revolutions including standard deviation.

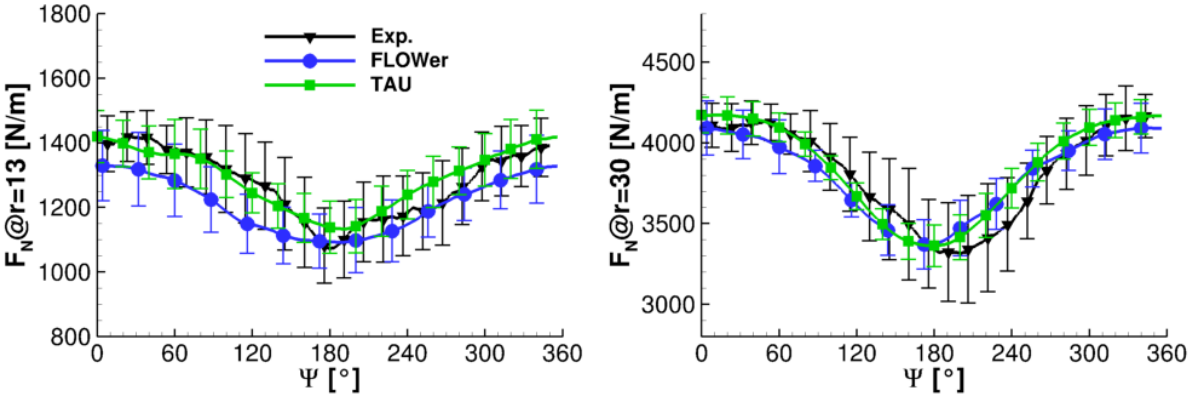

Figure 5: Normal force at 13m (left) and 30m (right) radius from experiment (black triangles), FLOWer (blue circles) and TAU (green squares) averaged over last 25 rotor revolutions including standard deviation.

intensity (which is not shown here for brevity) an excellent agreement can be observed.

The comparison of the normal force at 13m (left) and 30m (right) radius from the **rotor simulations** is depicted in Figure 5. As for the streamwise velocity and turbulent intensity the agreement with the experiment is excellent. Only for the outermost station (also not shown here for brevity) a strong phase shift is present in the experiment, but not in the simulations. Also the differences in the normal forces between the two codes are well in line with the predictions of the mean hub height velocity and turbulent intensity; i.e. the mean normal force in the TAU simulation is higher than in the FLOWer computation as for the mean hub height velocity. The same holds for the standard deviation and the turbulent intensity. Figure 4 illustrates the tangential force at the innermost blade section. Although this section represents the best agreement with the experiment among the four different sections, the largest mean to mean difference between TAU and the experimental results rise up to app. 15%, almost double compared to the difference between FLOWer and the experiment. Although this issue should be investigated in the future, it is of minor importance for the following work in this paper, since the normal force exerts a much bigger influence on the wake characteristics as the tangential force which will be investigated in the following section.

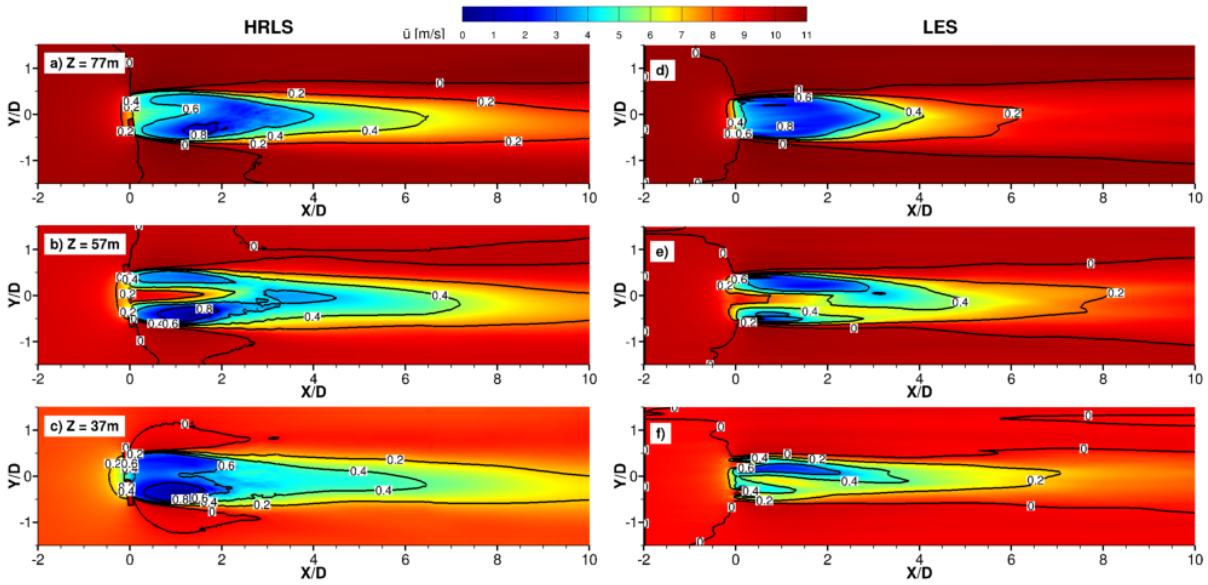

Figure 6: Mean streamwise velocity $\overline{u}(m/s)$ in three horizontal planes of the **validation case** at $z = 77$ m in a) and d), at $z = 57$ m in b) and e) and at $z = 37$ m in c) and f). The results for the HRLS (LES) are shown on the left (right). The axes are normalized by the rotor diameter $D = 80\ m$. The black contours represent the velocity deficit in the wake.

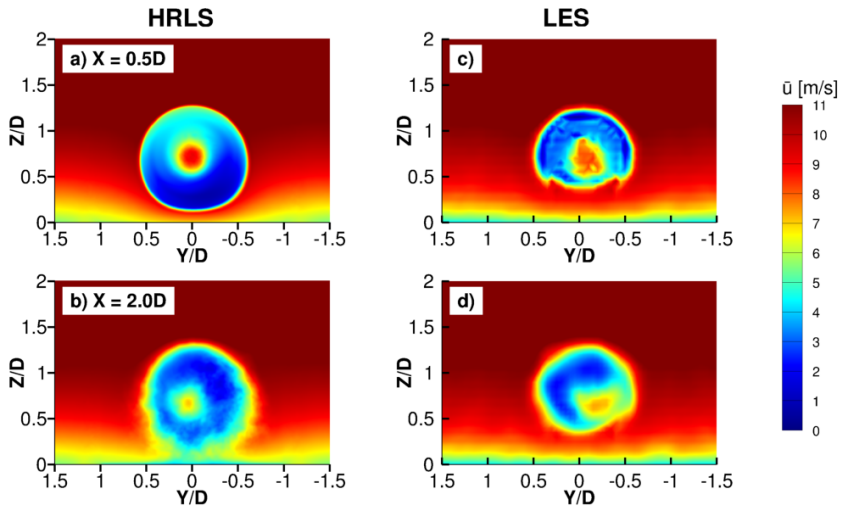

Figure 7: Mean streamwise velocity $\overline{u}(m/s)$ in two vertical planes of the **validation case** at $x = 0.5D$ in a) and c) and at $x = 2D$ in b) and d). The results for the HRLS (LES) are shown on the left (right). The axes are normalized by the rotor diameter $D = 80\ m$. The black circles in c) and d) represent the rotor area.

3.2. Wake Structures

The comparison of the wakes in the **validation case** in three horizontal planes (hub height + R/2, hub height and hub height - R/2) is depicted in Figure 6. As can be seen the overall agreement between the HRLS (a, b and c on the left) and LES (d, e and f on the right) is fair considering the fidelity of the different methods. While the velocity deficits on the upper plane (Figures 6a and d) indicated by the black lines and numbered labels are similar until $x/D = 3$,

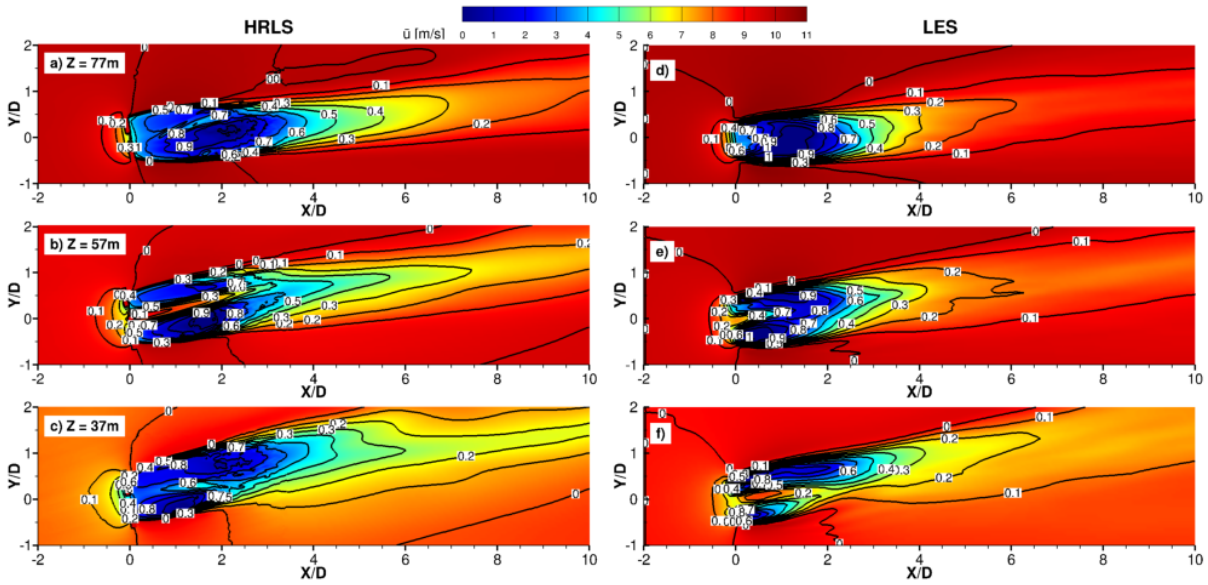

Figure 8: Mean streamwise velocity $\overline{u}(m/s)$ in three horizontal planes of the **nocturnal case** at $z = 77$ m in a) and d), at $z = 57$ m in b) and e) and at $z = 37$ m in c) and f). The results for the HRLS (LES) are shown on the left (right). The axes are normalized by the rotor diameter $D = 80\ m$. The black contours represent the velocity deficit in the wake.

larger differences at hub height (beneath the hub) in the near and the far wake can be seen in Figures 6b and e (c and f). A larger maximal velocity deficit of 0.8 can be seen in the near wake for the HRLS while it reaches only 0.6 in the LES. Differences are also apparent in the streamwise expansion of the wake. At hub height a velocity deficit of 0.4 (0.2) can be seen at $x/D = 7$ ($x/D = 10$) in the HRLS while it reaches only $x/D = 5$ ($x/D = 8$) in the LES. In conclusion, in the near wake a larger velocity deficit can be seen in the HRLS, resulting in a less rapid wake recovery in the HRLS in comparison to the LES.

The mean streamwise velocity in two vertical planes ($x = 0.5D$ and $x = 2D$) is compared in Figure 7. While the qualitative agreement wrt shape and position is good, the comparison of the absolute mean velocity reveals quantitative differences especially in the radial and azimuthal distribution, e.g. a very distinct deceleration can be observed in the LES at the blade tip reducing severely as one moves inboard. A second prominent difference occurs in the lower part of the rotor. At $x = 0.5D$ a minimal velocity of $\overline{u} = 2.0$ m s^{-1} can be seen in the lower part (upper part) of the rotor for the HRLS (LES). At $x = 2.0D$ a minimal velocity of $\overline{u} = 2.5$ m s^{-1} can be seen in the upper right (left) part of the rotor for the HRLS (LES). It has to be mentioned that the AD method has a low fidelity considering the near wake behind the rotor. In this part of the wake the HRLS leads to more precise results.

Figure 8 shows the wake behind the rotor in the **nocturnal case** in the same three horizontal planes. The overall agreement between the HRLS (left) and LES (right) regarding the deflection and the spanwise expansion is good. Due to the wind veer in the stably-stratified boundary layer the wake is not only convected downstream but also deflected in the spanwise direction. The deflection in the upper plane is small with approximately 5° (Figures 8a and d) and increases towards the ground reaching approximately 15° at the lower plane (Figures 8c and f) resulting in a skewed wake. The deflection in all three planes and also the shape of the wake are predicted similarly with both methods. Even the skewed double gaussian shape in the near wake in the lower plane can be observed well in both methods. The velocity deficit in the near wake is similar in both models with values for the HRLS of 0.9 (0.9, 0.8) at $Z = 77$ m and $x/D = 3$

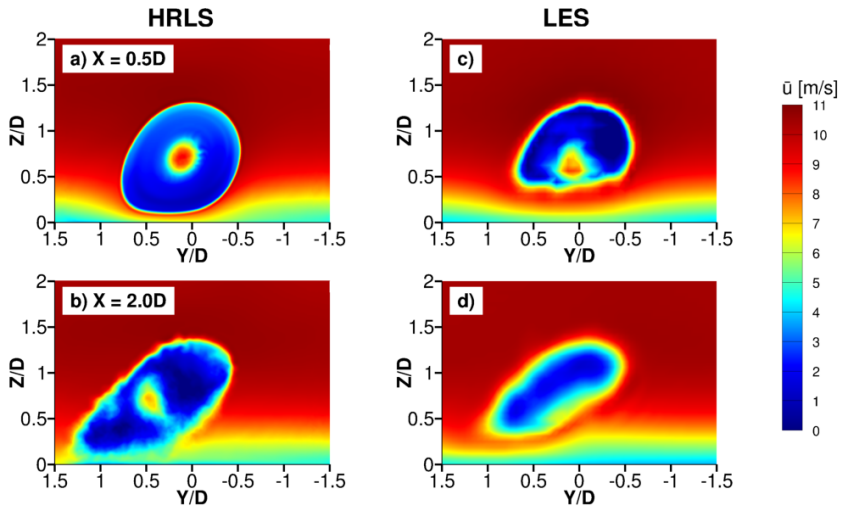

Figure 9: Mean streamwise velocity $\overline{u}(m/s)$ in two vertical planes of the **nocturnal case** at $x = 0.5D$ in a) and c) and at $x = 2D$ in b) and d). The results for the HRLS (LES) are shown on the left (right). The axes are normalized by the rotor diameter $D = 80\ m$.

($Z = 57$ m and $x/D = 2$, $Z = 37$ m and $x/D = 3$). The values for the LES are 0.9 (0.9, 0.8) at $Z = 77$ m and $x/D = 2$ ($Z = 57$ m and $x/D = 2$, $Z = 37$ m and $x/D = 2.5$). As in the previous case the streamwise wake extension differs. At hub height a velocity deficit of 0.2 is reached at $x/D = 10$ ($x/D = 6$) in the HRLS (LES).
The development of the wake one half and two diameters downstream of the rotor is shown in Figure 9. As in the previous case the deceleration in the LES is strongest in the upper rotor half and has almost disappeared in the lower half while the strongest deceleration in the HRLS is visible in the lower half (9a and c). Two diameters downstream the wake shows similar convection and distortion characteristics as can be seen in Figure 9b and d. The size of the wake differs, of course, due to the different streamwise extension of the wake.
In the proximity of the rotor the HRLS is able to resolve the velocities in the wake more precisely than the LES due to the higher fidelity of the method. However, the LES is able to simulate the far wake accurately with significantly less computational costs.

4. Conclusion

The work in the current paper presents the first important step towards the simulation of a resolved wind turbine rotor exposed to a real, non-neutral atmospheric boundary layer. At first the high fidelity approach (HRLS) is validated against the DanAero field experiment and the high fidelity setup used at IAG (Institute for Aerodynamics and Gasdynamics of the University of Stuttgart) using synthetic turbulent fluctuations. Both high fidelity approaches show excellent agreement among each other and compared to the experiment. Subsequently the DanAero rotor is exposed to a nocturnal atmospheric boundary layer of similar characteristics as the synthetic turbulence. Within this investigation the high fidelity simulations serve as a reference for comparison to an LES coupled with an AD, showing that the latter approach is capable of reproducing the overall flow field in the far wake but lacks the accuracy of predicting exact local velocity deficits in the near wake. A detailed investigation of the discrepancies between HRLS and LES is undergoing and will reveal further insight and possible improvements for lower fidelity models with the potential of significantly lower computational effort. While the HRLS were carried out in 768 hours on 1920 processors the LES needed 3h on 512 processors. It has to

be mentioned that with respect to computational performance the TAU code is not extremely well suited for this kind of application. The wall-clock time for the HRLS could be reduced by a factor of 10 with a well adopted code. Nevertheless the computational advantage of the LES is absolutely obvious. The integration of an actuator line approach in EULAG instead of the AD method will be the next step to increase the fidelity of the LES in the near wake. This will allow a detailed comparison of the near-wake region of both approaches and represent the next step towards a digital twin for research wind parks.

5. Acknoledgements

The authors would like to thank the DanAero project consortium for sharing the data on the DanAero turbine.

References

[1] Abkar M, Sharifi A and Porté-Agel F 2016 Wake flow in a wind farm during a diurnal cycle *J. Turbul.* **17**
[2] Bangga G, Lutz T, Jost E, Kramer E 2017 CFD studies on rotational augmentation at the inboard sections of a 10 MW wind turbine rotor. *J. Renew. Sustain. Energy* **9** 023304
[3] Bangga G and Lutz T 2021 Aerodynamic modeling of wind turbine loads exposed to turbulent inflow and validation with experimental data *J. Energy* **2**23 120076 https://doi.org/10.1016/j.energy.2021.120076
[4] Bangga G 2022 Consistency between Engineering Models and High Order Methods *Wind Turbine Aerodynamics Modeling Using CFD Approaches* (AIP Publishing LLC) 10.1063/9780735424111_008
[5] Englberger A and Dörnbrack A 2018 Impact of the Diurnal Cycle of the Atmospheric Boundary Layer on Wind-Turbine Wakes: A Numerical Modelling Study *Boundary-Layer Meteorol.* **1**66
[6] Knopp T 2006 Model-consistent universal wall-functions for RANS turbulence modelling *Proc. Intern. Conf. BAIL*
[7] Kroll N, Rossow C C, Becker K, Thiele F 200 The megaflow project *Aerospace Science and Technology* **4**
[8] Löwe J, Probst A, Knopp T and Kessler R 2016 Low-Dissipation Low-Dispersion Second-Order Scheme for Unstructured Finite-Volume Flow Solvers *AIAA Journal* **5**4
[9] Menter F R 1994 Two-Equation Eddy-Viscosity Turbulence Models for Engineering Applications *AIAA Journal* **3**2
[10] Mirocha J D, Kosovic B, Aitken M L, Lundquist J K 2015 Implementation of a generalized actuator disk wind turbine model into the Weather Research and Forecasting model for large-eddy simulation applications *J. Renew. Sustain. Energy* **6**
[11] Probst A, Löwe J, Reuß S, Knopp T and Kessler R 2016 Scale-Resolving Simulations with a Low-Dissipation Low-Dispersion Second-Order Scheme for Unstructured Flow Solvers *AIAA Journal* **5**4
[12] Prusa J M, Smolarkiewicz P K and Wyszogrodzki A A 2008 EULAG, a computational model for multiscale flows *Comput. Fluids* **3**7
[13] Schepers J G et al. 2021 IEA Wind TCP Task 29 Phase IV: Detailed Aerodynamics of Wind Turbines *Zenodo* [https://doi.org/10.5281/zenodo.4813067]
[14] Schwamborn D, Gerhold T and Heinrich R 2006 The DLR TAU-Code: Recent Applications in Research and Industry *ECCOMAS CFD*
[15] Shur M L, Spalart P R, Strelets M K and Travin A K 2008 A Hybrid RANS-LES Approach with Delayed-DES and Wall-Modelled LES Capabilities *Intern. J. of Heat and Fluid Flow* **2**9
[16] Smolarkiewicz P and Margolin L 1997 On Forward-in-Time Differencing for Fluids: an Eulerian/Semi-Lagrangian Non-Hydrostatic Model for Stratified Flows *Atmosphere-Ocean* **3**5
[17] Troldborg N, Bak C, Aagaard Madsen H and Skrzypinski W R 2013 DANAERO MW: Final Report DTU Wind Energy E No. 0027(EN)
[18] Troldborg N, Sørensen J N, Mikkelsen R, Sørensen N N 2014 A simple atmospheric boundary layer model applied to large eddy simulations of wind turbine wakes *Wind Energy* **17**
[19] Vollmer L, Steinfeld G, Heinemann D, Kühn M 2016 Estimating the wake deflection downstream of a wind turbine in different atmospheric stabilities: an LES study *Wind Energy Sci.* **1**
[20] Wenz F, Maas O, Arnold M, Lutz T, Krämer E 2023 Assessment of low-frequency aeroacoustic emissions of a wind turbine under rapidly changing wind conditions based on an aero-servo-elastic CFD simulation *Wind Energy* **2**6